Developmental Biology
Stem Cells and Regenerative Medicine

Stochastic cell-intrinsic stem cell decisions control colony growth in planarians

Reviewed Preprint
v1 • November 1, 2024
Not revised

Tamar Frankovits, Prakash Varkey Cherian, Yarden Yesharim, Simon Dobler, Omri Wurtzel

The School of Neurobiology, Biochemistry & Biophysics, George S. Wise Faculty of Life Sciences, Tel Aviv University, Tel Aviv, Israel • Interfaculty Institute of Microbiology and Infection Medicine, University of Tübingen, Tübingen, Germany • Sagol School of Neuroscience, Tel Aviv University, Tel Aviv, Israel

https://en.wikipedia.org/wiki/Open_access
Copyright information

eLife Assessment

This manuscript establishes a mathematical model to estimate the key parameters that control the repopulation of planarian stem cells after sublethal irradiation as they undergo fate-switching as part of their differentiation and self-renewal process. The findings are **valuable** for future investigation of stem cell division in planarians. The methods are **solid**, integrating modeling with perturbations of key transcription factors known to be critical for cell fate decisions, but the authors have only shown that this is the case for a small number of stem cell types.

https://doi.org/10.7554/eLife.100885.1.sa3

Abstract

Stem cells contribute to organismal homeostasis by balancing division, self-renewal and differentiation. Elucidating the strategies by which stem cells achieve this balance is critical for understanding homeostasis, and for addressing pathogenesis associated with the disruption of this balance (e.g., cancer). Planarians, highly regenerative flatworms, use pluripotent stem cells called neoblasts to maintain and regrow organs. A single neoblast can rescue an entire animal depleted from stem cells and regenerate all cell lineages. How neoblast differentiation and clonal expansion are governed to produce all the required cell types is unclear. Here, we integrated experimental and computational approaches to develop a quantitative model revealing basic principles of clonal growth of individual neoblasts. By experimentally suppressing differentiation to major lineages, we elucidated the interplay between colony growth and lineage decisions. Our findings suggest that neoblasts pre-select their progenitor lineage based on a cell-intrinsic fate distribution. Arresting differentiation into specific lineages disrupts neoblast proliferative capacity without inducing compensatory expression of other lineages. Our analysis of neoblast colonies is consistent with a cell-intrinsic decision model that can operate without memory or communication between neoblasts. This simple cell fate decision process breaks down in homeostasis, likely because of the activity of feedback mechanisms. Our findings uncover essential principles of stem cell regulation in planarians, which are distinct from those observed in many vertebrate models.

These mechanisms enable robust production of diverse cell types, and facilitate regeneration of missing tissues.

Introduction

Stem cells are crucial for achieving and maintaining homeostasis. Paradoxically, they contribute to an organism's equilibrium through highly dynamic behavior, continuously balancing their population size by regulating rates of self-renewal and differentiation. Understanding the strategies used to accomplish this balance can provide the key to elucidating organismal homeostasis, as well as to modeling pathogenesis associated with disruption to this balance (e.g., cancer) (Passegué et al., 2003; Singh et al., 2011).

Valuable insights into stem cell behavior can be derived from studying systems that rely on principles differing significantly from those characterizing vertebrate stem cells. Neoblasts, the pluripotent stem cells in planarians, function in tissue regeneration and maintenance, providing an intriguing platform in this regard. Neoblasts avoid quiescence, and quickly adapt to changes in organismal requirements by adjusting the quantities and types of cells they produce (González-Estévez et al., 2012; Wagner et al., 2011). These strategies challenge fundamental concepts of vertebrate stem cells. For example, in adult vertebrates, hematopoietic stem cells typically divide slowly, giving rise to rapidly dividing transit amplifying cells forming tissue-specific progenitors (Abkowitz et al., 2000; Becker et al., 2006). These progenitors bear the primary responsibility for maintaining homeostasis. Planarian neoblasts, by contrast, divide rapidly and do not employ transit amplifying cells for progeny production (Pearson, 2022; Raz et al., 2021; van Wolfswinkel et al., 2014). Moreover, neoblasts do not seem to retain memory of the progeny cell types they generate (Raz et al., 2021; van Wolfswinkel et al., 2014). Notably, despite being essentially ageless and immortal, neoblasts do not display cancerous-like states (Van Roten et al., 2018). Therefore, elucidating how neoblasts balance self-renewal and differentiation can contribute to understanding fundamental strategies that facilitate tissue homeostasis and regeneration of lost or damaged tissues (Levin et al., 2019).

Prior modeling of neoblast dynamics in planarians has produced a valuable analytical framework for studying the dynamics of the entire neoblast system (Mangel et al., 2016). However, analyzing isolated neoblasts and their progeny can be instrumental for understanding how decisions are made at a single cell resolution, as well as for deriving physiological parameter values (e.g., corresponding to proliferation and differentiation) that are relevant to the larger system. *In vivo* analysis of individual neoblasts and their progeny is often achieved by applying subtotal irradiation to whole planarians, which results in near-complete neoblast ablation (Wagner et al., 2011). Surviving neoblasts proliferate to form distinct colonies, allowing analysis of growth dynamics and progeny identity (Lei et al., 2016; Wagner et al., 2012). Though such analysis has been instrumental in uncovering regulators of proliferation and differentiation (Wagner et al., 2012), a quantitative analysis of neoblast colony growth that integrates these principles has yet to be established and experimentally validated.

Several open questions need to be addressed in the development of such a model. For example, it is unclear whether neoblasts select their lineage identity in a synchronous manner or function independently (Bohr et al., 2021; Reddien, 2018). Moreover, as indicated above, it is unclear whether neoblasts maintain memory of their decisions over successive rounds of the cell cycle (Pearson, 2022). In addition, as discussed in what follows, critical knowledge is lacking regarding the ability of neoblasts to switch from producing differentiating lineage to contributing to neoblast colony growth; an understanding of this switch is fundamental for analyzing the overall development of a colony, and for describing new tissue production in regeneration.

Herein, we begin to address these gaps, integrating experimental and computational approaches to analyze neoblast colony growth. Our analysis does not assume communication between neoblasts or memory of cell fate decisions; rather, it explores whether straightforward stochastic selection of division outcome can adequately describe the growth of a neoblast colony. Based on *in vivo* analysis of neoblast clone growth, neoblast division can result in three potential outcomes (**Fig 1**) (Lei et al., 2016; Raz et al., 2021): (1) symmetric renewal, which generates two neoblasts; (2) symmetric differentiation, which generates two post-mitotic cells; and (3) asymmetric division, which produces a neoblast and a post-mitotic cell.

In what follows, we study and analyze colony growth based on these principles. We derive key parameter values from experimental data and show that these values predict colony growth with high accuracy. Next, in a series of experiments, we seek to uncover whether the core principles that drive neoblast colony growth (as proposed in our model) are further shaped by individual neoblasts' decisions regarding progeny lineage commitment. In particular, many S/G2/M neoblasts express fate-specifying transcription factors (FSTFs), which direct the differentiation of their progeny into specific lineages (Reddien, 2013; Scimone et al., 2014; Zeng et al., 2018). Importantly, a neoblast can express different FSTFs in successive rounds of division, which results in production of post-mitotic progenitors of different lineages (Raz et al., 2021; van Wolfswinkel et al., 2014). Thus, the growth potential of the colony is not compromised by FSTF expression. Yet, it remains unclear how the growth of a colony might be affected when expression of a particular FSTF (and thus the corresponding cell lineage) is blocked: for example, does colony growth remain stable, with other lineages being overexpressed to compensate for the blocked lineage? Notably, our experimental perturbation analysis shows that blocking the expression of an FSTF incapacitates a proportion of neoblasts equivalent to the size of the lineage affected. This observation reveals a critical dependency: once a neoblast commits to a specific lineage, it retains this identity until cell division concludes. By contrast, inhibiting FSTFs during homeostasis resulted in an increase in the number of cycling cells, consistent with an activity of feedback mechanisms that regulate cell proliferation in homeostasis (Cheng et al., 2018; Pearson and Sánchez Alvarado, 2010).

Together, our findings imply that simple design principles govern cell fate choices in neoblast colonies, and that accurate prediction of colony growth does not require assumptions of fate-specification memory, or coordination of cell fate choices between neoblasts. Moreover, our findings suggest that all neoblasts in a colony are functionally equivalent (i.e., able to self-renew and to divide to all cell types), and elucidate the contribution of decisions in individual planarian stem cells to achieving systemic homeostasis.

Results

Analysis of neoblast colony growth

Following subtotal irradiation, a surviving neoblast may proliferate to form a colony (**Fig 2A**). The growing colony is the exclusive source of new cells (Wagner et al., 2012, 2011). We used an exponential growth equation to estimate the change in colony size over time of a successfully established colony by a surviving neoblast (Eq 1). The function incorporates three parameters to estimate colony growth: (1) average cell cycle length (τ); (2) symmetric renewal probability (p), where symmetric renewal rate per hour is $p' = p/\tau$; and (3) symmetric differentiation or neoblast elimination probability (q), where symmetric differentiation or neoblast elimination rate per hour is $q' = q/\tau$. Asymmetric divisions do not alter neoblast count (**Fig 1**).

$$\frac{dN}{dt} = p'N - q'N = \frac{(p-q)N}{\tau} \quad [1]$$

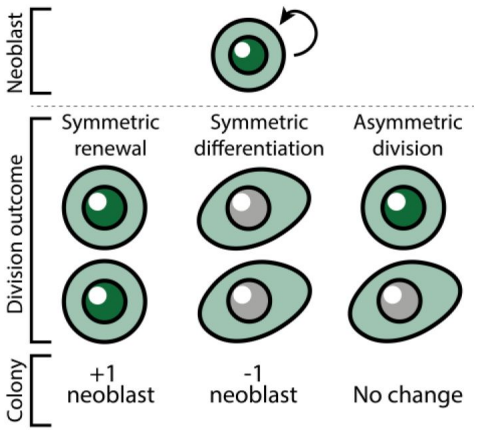

Figure 1.

Potential outcomes of neoblast division and the effect on colony size

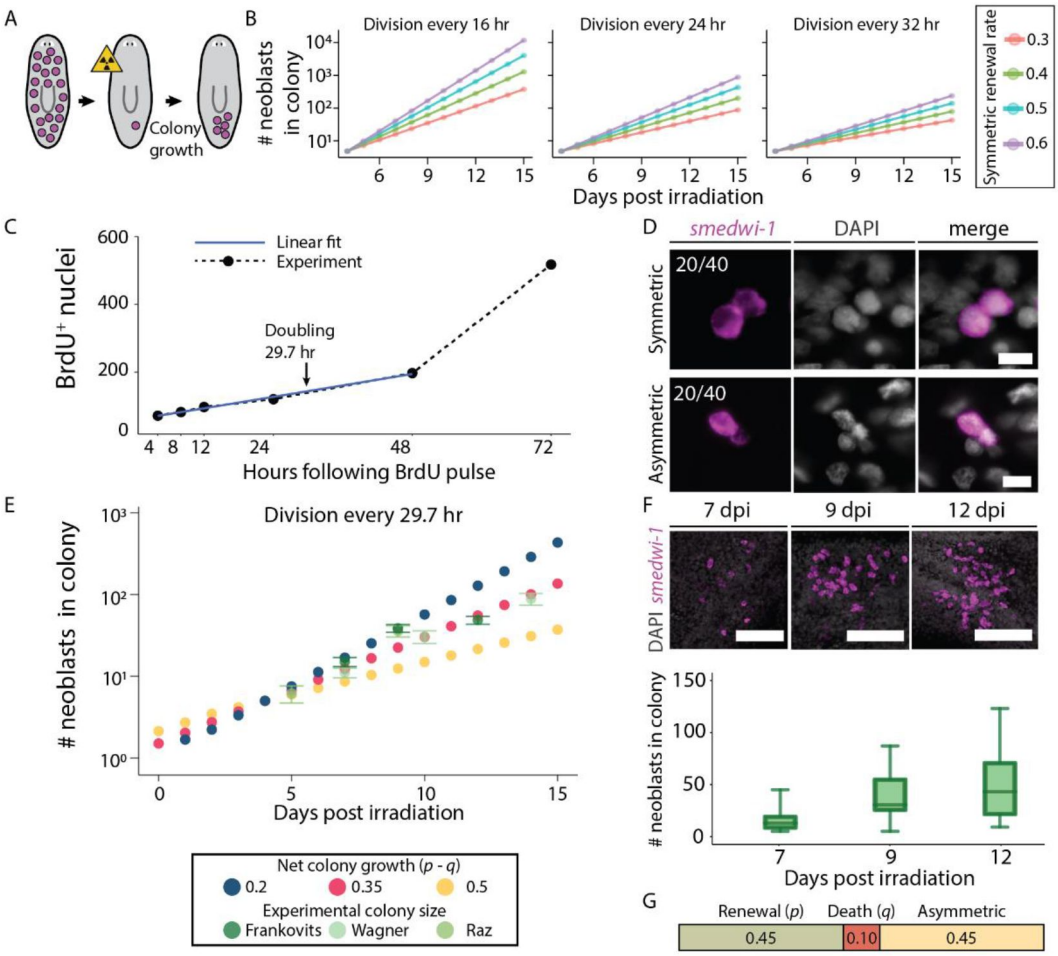

Figure 2.

Parameters determining neoblast colony size.

(A) Outline of colony growth following subtotal irradiation. Planarians are irradiated to eliminate all neoblasts (purple dots) except for a single survivor. The surviving neoblast forms a proliferating neoblast colony. (B) The impact of average cell cycle length (τ) and probability of symmetric renewal division (*p*) on colony size is shown (*q* was set to 0). (C) Re-analysis of BrdU incorporation time series (Lei et al., 2016) in expanding planarian colonies was used for determining the average cell cycle length (Methods). Linear regression (blue line; y = 59.77 + 2.81 * t; Pearson r = 0.997) was used to identify the doubling time of the colony, and was determined as 29.7 hours (black arrow). (D) The fraction of symmetric renewal divisions was estimated by examining neoblast pairs in colonies (Methods). Scale = 10 μm. (E) The impact of symmetric differentiation or neoblast elimination on colony size was tested, assuming a 29.7 hour long cell cycle. Experimental data of colony sizes at different time points were overlaid to determine the value of biologically relevant parameter. Frankovits data collected here; Wagner, reanalysis (Wagner et al., 2012); Raz, reanalysis (Raz et al., 2021). Error bars show the standard error. (F) Shown are neoblast colonies at three time points following subtotal irradiation. Representative images (z-projection) are shown (top), and neoblast counting of different colonies is shown (box indicates interquartile range; whiskers show range; horizontal bar indicates median). Scale = 100 μm. (G) The estimated fractions of divisions leading to symmetric renewal, symmetric differentiation or elimination, and asymmetric divisions.

We used the solution to the equation, and included the initial colony size (*N*0), to predict colony sizes (Eq 2) using a range of parameter values and evaluated the model predictions (**Fig 2B**; **Fig S1**) with our own and published data (Raz et al., 2021; Wagner et al., 2012).

$$N(t) = N_0 e^{\frac{(p-q)t}{\tau}} \quad [2]$$

The plots in **Figure 2B** show how varying the value of growth parameters is predicted to affect colony size. The cell division time (τ) has the most substantial impact on colony growth. For example, a simulated colony with a fast (16 hours) cell cycle (with p and q set at 0.5 and 0, respectively) had a neoblast count approximately ten times larger than that reported in literature (Lei et al., 2016; Raz et al., 2021; Wagner et al., 2012, 2011; Zeng et al., 2018). To determine the average cell cycle time (τ), we re-analyzed available colony growth data that had previously been experimentally obtained using bromodeoxyuridine (BrdU) metabolic labeling (Lei et al., 2016). In those experiments, BrdU was incorporated into DNA during both symmetric and asymmetric divisions using a pulse (4 hours) significantly shorter than the cell cycle time, followed by a chase of up to 72 hours (**Fig 2C**). We predicted that the $BrdU^+$ cell number would grow linearly until the entire population doubles. Then, completion of successive cell divisions would lead to exponential growth in $BrdU^+$ cell number. Indeed, the colony growth was initially linear (Pearson r = 0.997), and using linear regression, we estimated that the colony doubling time, and hence the average cell cycle length, was 29.7 hours (**Fig 2C**).

The symmetric renewal probability (p) is a vital factor in colony growth, and even slight variations in p have large cumulative effects (**Fig 2B**). We experimentally determined the symmetric renewal probability by subjecting planarians to subtotal irradiation (1750 rad; Methods) and identifying neoblasts via fluorescence *in situ* hybridization (FISH) with the *smedwi-1* marker (Reddien et al., 2005b), a pan-neoblast marker. We imaged pairs of adjacent *smedwi-1*$^+$ cell in the colony, and classified the *smedwi-1*$^+$ cell pairs based on their *smedwi-1* expression levels: high-level pairs indicated symmetric renewal, while pairs with one high and one low *smedwi-1*$^+$ cell categorized as asymmetric division (**Fig 2D**). By analyzing 40 dividing pairs we estimated that 50% of divisions that produce at least one neoblast are symmetric renewal divisions, in agreement with previous findings (Lei et al., 2016; Raz et al., 2021).

The value of q, representing symmetric differentiation and neoblast loss probability (Raz et al., 2021), also plays a role in colony dynamics (**Fig 2E**, S1B). Yet the value of this parameter is more difficult to estimate experimentally (e.g., naïve measurement of cell death using TUNEL in irradiated planarians would be insufficient, because cell death is not limited to neoblasts). We analyzed the effect of different neoblast elimination probabilities on colony size (**Fig 2E**; **Fig S1B-E**), and compared the estimates of the analysis with colony size in our experimental data and by extracting colony size measurements from published literature (**Fig 2E-F**; Methods) (Raz et al., 2021; Wagner et al., 2012, 2011). Considering an average cell cycle length of 29.7 hours, the experimental data indicated that the average colony size was affected by symmetric differentiation or loss probability (q), estimated at ~10% of the neoblasts in each cycle (**Fig 2E**, **Fig S1B-E**). Given the values derived for q, we can conclude that symmetric renewal (p) and asymmetrically dividing neoblasts each account for 45% of cell divisions (**Fig 2G**; Methods).

In vivo, we observed a large variation in the size of the colonies at each time point (**Fig 2F**). This could be a consequence of an altered delay between irradiation and the onset of colony growth, or from a stochastic decision to undergo symmetrical or asymmetrical division in the early colony. Despite this variability, the observed exponential growth suggested a steady proliferation rate once the colony founding neoblast recovered at day four (**Fig 2E**, S1A).

Inhibition of lineage differentiation reduces neoblast colony size

Regulating growth and homeostasis requires balancing self-renewal and progeny production. To better understand how neoblasts maintain this balance, we focused on the interplay between the overall growth of the colony and the ability of individual neoblasts to express FSTFs, which are required for specific progeny production (Scimone et al., 2014). More specifically, we investigated how inhibiting differentiation into specific lineages, by suppressing FSTF expression, influences colony size. Considering the linear correlation between post-mitotic progeny production and neoblast number (van Wolfswinkel et al., 2014; Wagner et al., 2012), we hypothesized three potential outcomes (**Fig 3A**) and their probable effects on symmetric renewal (*p*) and symmetric differentiation or elimination (*q*): (1) Unchanged: *p* and *q* remain balanced, resulting in no change in colony size. This outcome would suggest that the balance of self-renewal and progeny generation is preserved through compensatory production of alternative cell types when differentiation to a specific lineage is suppressed. (2) Larger: An increase in *p*, leading to larger colonies, possibly due to fewer asymmetric divisions in the blocked lineage. (3) Smaller: An increase in *q*, leading to smaller colonies, possibly because neoblasts committed to the blocked lineage have become dysfunctional. We used published frequencies of three major lineages (epidermis, intestine, and *foxF-1*$^{+}$ neoblasts) to estimate the size of the colony in each of the described scenarios (**Fig 3A**) (Raz et al., 2021; Scimone et al., 2018, 2014; van Wolfswinkel et al., 2014). Theoretically, inhibiting a predominant lineage, such as the epidermal lineage (28%), may significantly affect colony size, which could be observed experimentally, whereas changes in colony size following inhibition of smaller lineages could be difficult to distinguish within the experimental time scale.

On the basis of this assumption, we inhibited differentiation into the epidermal lineage after subtotally irradiating planarians. Following a four-day recovery after subtotal irradiation, we suppressed the FSTF *zfp-1*, which is critical for production of differentiating epidermal progenitors (**Fig S2**) (Cheng et al., 2018; Tu et al., 2015; van Wolfswinkel et al., 2014; Wagner et al., 2011), but does not impact directly other lineages (van Wolfswinkel et al., 2014). Then, we evaluated neoblast colony sizes in *zfp-1*-suppressed (*zfp-1* (RNAi)) planarians at three time points (7, 9, and 12 days post-irradiation; dpi), and compared them with control colony sizes (**Fig 3B**, Methods). Initially (7 dpi), colony sizes were similar. However, at 9 dpi, *zfp-1* (RNAi) colonies were significantly smaller than in controls. Moreover, unlike in controls, *zfp-1* (RNAi) colonies showed no additional growth, on average, during the period between 9 dpi and 12 dpi, though there was a slight increase in the median colony size (**Fig 3B**).

Our basic assumption was that reduction in colony size (vs. control) following *zfp-1* inhibition would indicate an increase in symmetric differentiation or elimination (*q*). However, an alternative possibility is that *zfp-1* inhibition causes mitotic arrest in neoblasts—which would prevent proliferation but would not necessarily result in cell death. We tested whether *zfp-1* (RNAi) colonies had a lower number of cycling neoblasts. We detected neoblasts in mitosis using immunofluorescence (IF) with an anti-H3P-antibody (**Fig 3C**; Methods). We found that control colonies did not significantly differ from *zfp-1* (RNAi) colonies in the number of H3P^{+} cells, either in absolute numbers or normalized to average neoblast counts in colonies (Methods). This result suggested that FSTF inhibition did not cause a general mitotic arrest. Further analysis with 2'-Deoxy-2'-fluoro-5-ethynyluridine (EdU) labeling (**Fig 3D**; Methods) showed a substantial decrease in EdU^{+} nuclei in *zfp-1* (RNAi) animals (vs. controls), indicating reduced new cell production. However, normalizing EdU^{+} nuclei to average colony size (**Fig 3D**; Methods) revealed a comparable proportion of cells entering S-phase. Given the unchanged ratios of cycling and mitotic cells, we can conclude that the diminished colony size following *zfp-1* suppression is indeed likely to result either from increased symmetric differentiation or neoblast elimination (*q*). We further suggest that neoblast elimination is a more plausible explanation than increased symmetric differentiation: If *zfp-1* suppression were to lead to increased symmetric differentiation, we would expect to observe a noticeable decline in the number of neoblasts within

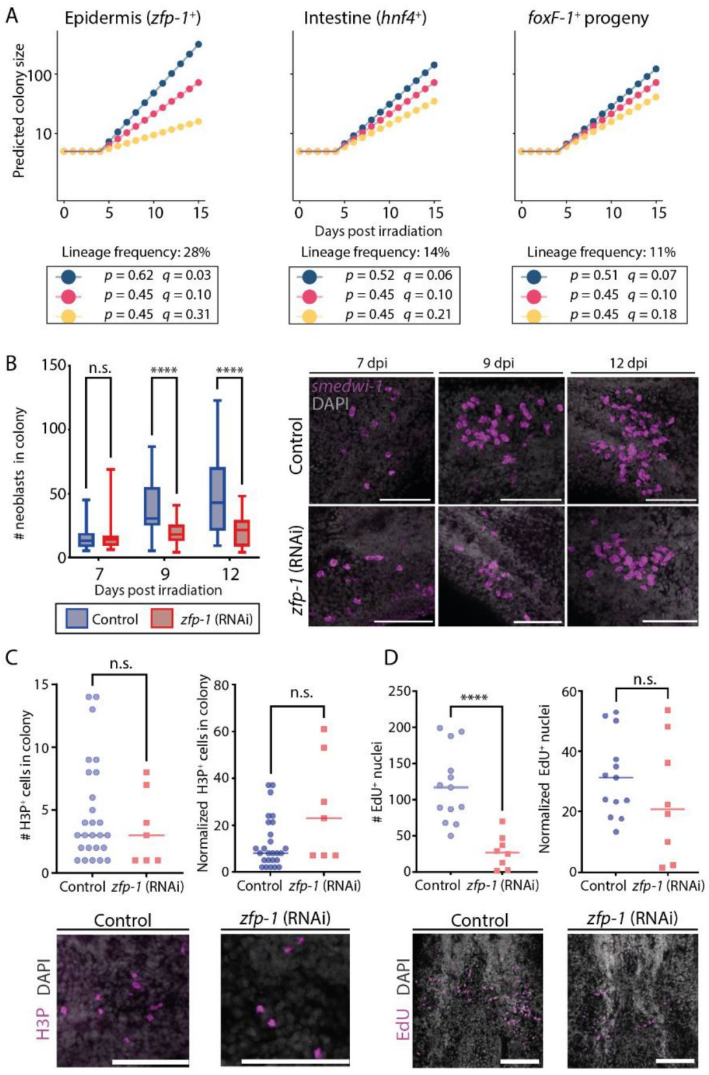

Figure 3.

Reduced neoblast colony size following lineage specification block.

(A) Models for lineage growth. Potential outcomes of lineage inhibitions were assessed by altering the colony growth and degradation parameters. Applying known lineage frequencies (Raz et al., 2021) to the models indicated that inhibiting production of a major lineage could dramatically impact colony size (left, epidermis). By contrast, inhibition of smaller lineages (middle, right) might have a smaller impact, which would be difficult to detect (Blue: increase in symmetric renewal; red: unchanged renewal and degradation; yellow: increase neoblast degradation). Growth was calculated using the following values: *N0* = 5, τ = 29.7 hr, and growth lag time of 5 days (Raz et al., 2021; Wagner et al., 2012). (B) Shown are counts (left) of neoblasts in colonies at three time points following irradiation, which was followed by inhibition of *zfp-1* or control by RNAi. Lineage inhibition resulted in a highly significant decrease in colony size at later time points (box indicates interquartile range (IQR), whiskers show range, bar indicates the median). Number of control colonies analyzed at 7 dpi n = 28; at 9 dpi n = 30; at 12 dpi n = 30; Number of *zfp-1* (RNAi) colonies analyzed at 7 dpi n=15; at 9 dpi n=30; at 12 dpi n = 30. Representative colonies (z-projection) are shown (right). (C) Comparison of absolute (top-left) or normalized (top-right) $H3P^+$ cell number in *zfp-1* (RNAi) and control colonies showed a non-significant difference (Methods). Representative H3P labeling images are shown (Bottom). Importantly, the number of detectable $H3P^+$ cells was small. (D) Comparison of (top-left) EdU^+ nuclei in *zfp-1* (RNAi) and control colonies showed a significant reduction, contributing to the smaller colony size. Comparison of normalized EdU^+ nuclei numbers (top-right) showed a non-significant difference, indicating that a similar proportion of neoblasts in the colony were cycling (Methods). Representative EdU labeling images (z-projection) are shown (Bottom). Statistical significance was assessed using Mann-Whitney two-tailed test (Methods). n.s., not significant, **** $P < 0.0001$. Scale = 100 µm.

colonies, while proliferation rates remained stable. Yet, the non-significant difference in EdU-labeling (**Fig 3D**) between *zfp-1* (RNAi) and control colonies suggested that inhibition of the FSTF *zfp-1* likely led to increased neoblast elimination.

Specialized neoblasts are produced in *zfp-1* (RNAi) colonies

Building upon our findings regarding lineage-specific inhibition effects, we next investigated how RNAi of *zfp-1* affected the prevalence of other specialized neoblasts in colonies. We hypothesized that if neoblast elimination was the primary effect of *zfp-1* inhibition, we would observe an absolute decrease in specialized neoblasts of other lineages (e.g., intestine), but not necessarily a relative decrease. We used subtotal irradiation, and following recovery we inhibited *zfp-1*. Then, we counted specialized neoblasts expressing intestine lineage markers (Scimone et al., 2014; Wagner et al., 2011), and *tgs-1* (Raz et al., 2021; Zeng et al., 2018), which is suggested to label neural progenitors (**Fig 4A-B**; Methods). Both control and *zfp-1* (RNAi) colonies contained specialized neoblasts. Notably, a decrease in intestine specialized neoblasts was detectable, aligned with the reduced colony size (**Fig 4A**). Small numbers of *tgs-1*$^{+}$ neoblasts were observed, with no significant reduction in their counts (**Fig 4B**). Together, these results suggested that specialized neoblasts were produced in *zfp-1* (RNAi) colonies, but that production of other (non-suppressed) lineages did not increase. This indicated that neoblast elimination predominantly accounts for the reduction in colony size following suppression of the epidermal lineage, without compensation by overproduction of other lineages.

To further analyze the impact of *zfp-1* inhibition on colony growth, we examined the numbers of neoblasts in 64 control colonies and in 53 *zfp-1* (RNAi) colonies, at 12 dpi (**Fig 4C-D**). The proportion of colonies containing five or more neoblasts was greater in the control group (75%) than in the *zfp-1* (RNAi) group (45%; Fisher's exact test two-tailed $P = 0.001$). Importantly, more *zfp-1* (RNAi) animals failed to develop colonies compared to controls (55% and 25%, *zfp-1* (RNAi) and control colonies, respectively). This might have resulted from the stochastic selection of a *zfp-1* identity by the neoblasts that initially established the colony, and which led to their further dysfunction, and was therefore detrimental to the development of the colony.

Simulation of colony growth following *zfp-1* inhibition

We developed a simulation to recapitulate the observed reduction in colony growth following *zfp*-1 inhibition. Our simulation methodology was designed to mimic real-world neoblast dynamics under *zfp-1* inhibition in a colony, using empirically derived probabilities for each cell cycle outcome. First, we randomly sampled initial colony sizes from the set counted at 7 dpi (**Fig 3B**). In every simulation cycle, each neoblast fate was selected based on the probabilities of cell cycle outcomes identified above, derived from empirical data (symmetric renewal, asymmetric division, symmetric differentiation or elimination; **Fig 2G**). The change in colony size was calculated over approximately six cell cycles. We conducted 100 iterations per simulation and compared the results with experimental data (**Fig 4E**; Methods). The simulated colony sizes closely matched the experimental observations. When simulating *zfp-1* (RNAi) colony growth by increasing the symmetric differentiation or elimination probability (q) by the known proportion of *zfp-1*$^{+}$ neoblasts, the model recapitulated the experimental findings (**Fig 4E-F**). Notably, many simulated *zfp-1* (RNAi) colonies failed to grow, often because of initial sampling of a state of symmetric differentiation or elimination, prohibiting further development of the colony (**Fig 4F**).

The agreement of these simulations with the experimental results is aligned with a model where neoblasts independently select their cell cycle outcome based on a replication outcome distribution without maintaining any memory of previous replication outcomes. Moreover, inhibition of a gene required for neoblast differentiation (e.g., FSTF) impedes the contribution of neoblasts that randomly selected this identity from any further contribution to colony growth across the timescale of the simulation.

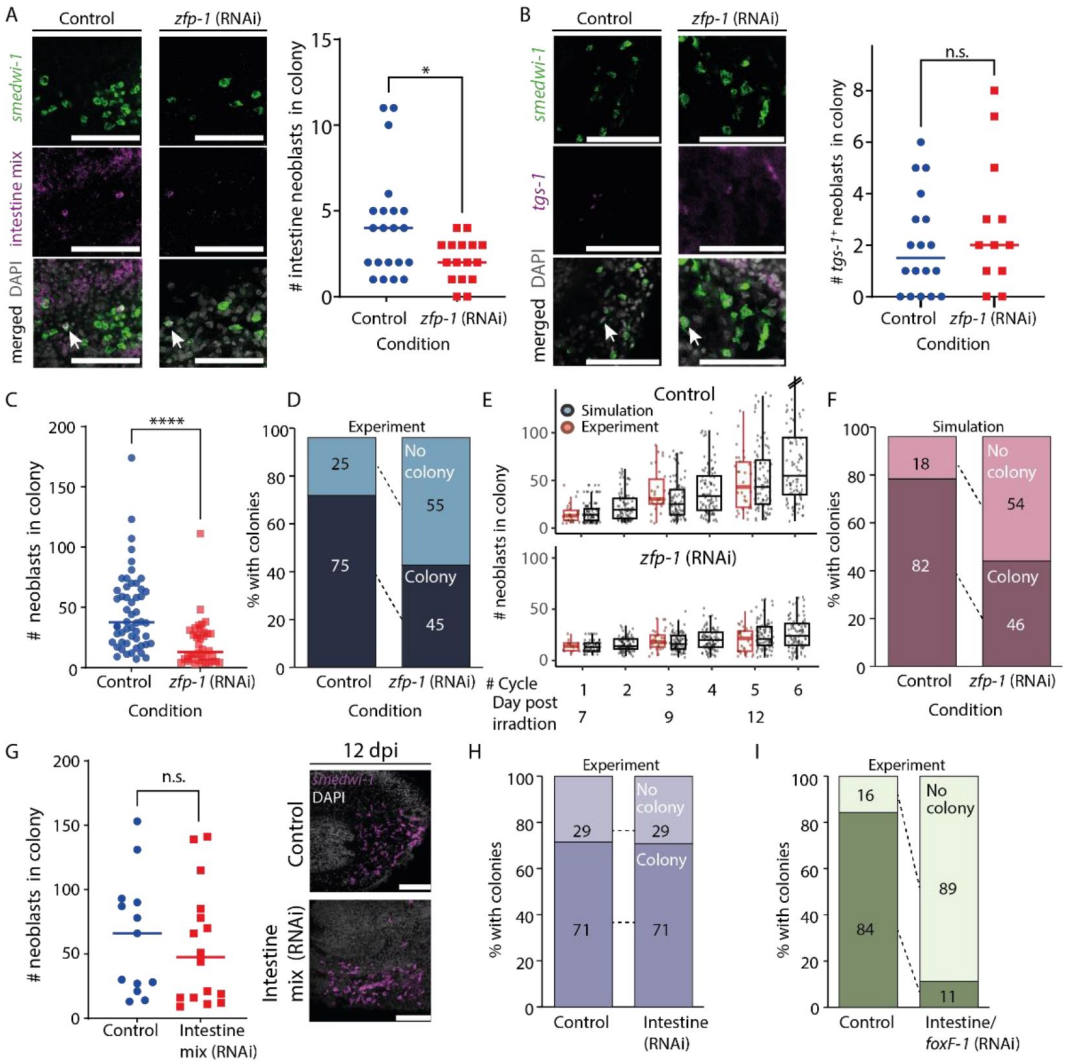

Figure 4.

Simulation of neoblast colony growth following lineage block.

(A-B) Neoblasts expressing lineage gene expression markers were detected using FISH (intestine mix: *hnf-4, gata4/5/6,* and *nkx2.2*; *tgs-1*), and were counted in colonies of control and *zfp-1* (RNAi) animals at 12 dpi (Methods). Left panels show confocal images of representative colonies (Methods); quantification of the experiment is shown on the right. Scale= 100 µm. (C) Comparison of colony size in control and in *zfp-1* (RNAi) animals 12 dpi showed a highly significant reduction in the size of *zfp-1* (RNAi) colonies (Mann-Whitney two-tailed test, **** $P < 0.0001$). Data is also shown in **Fig 3B**. (D) Summary of colony production in control and *zfp-1* (RNAi) animals based on analysis of 64 and 53 control and *zfp-1* (RNAi) colonies, respectively, at 12 dpi. Developed: ≥ 5 neoblasts detected; No colony < 5 neoblasts detected. (E) Simulation of colony growth in control and *zfp-1* (RNAi) animals, bottom and top, respectively (Methods). Shown are multiple iterations (black dots; n = 100 for each condition) of colony size simulation starting at 7 dpi. Experimental data quantifying colony sizes are shown (red dots) next to the corresponding simulation cycle. Box indicates the IQR; whiskers indicate ±1.5 x IQR; values out of the whisker range (outliers) were removed for clarity. (F) Summary of colony production in simulated control and *zfp-1* (RNAi) animals based on experimentally determined lineage frequencies, and assuming no memory in division outcome decision. Developed colony: ≥ 5 neoblasts in the simulation on day 12. (G) Neoblasts were counted in colonies 12 dpi, which was followed by inhibition of intestine progenitors by combined RNAi treatment (*hnf-4*, *gata4/5/6*, *nkx2.2*). Lineage inhibition did not affect colony size (left). Representative colonies (z-projection) are shown (right). Scale = 100 µm. (H-I) Summary of colony establishment in control and RNAi animals. (H) Suppression of intestine lineage did not affect the likelihood of producing colonies (n = 21 and 24, control and RNAi animals, respectively). (I) Combined suppression of *foxF-1* (Scimone et al., 2018) and intestine lineage production resulted in a significant reduction in the likelihood of producing colonies (Fisher's exact test two tailed $P = 4 \times 10^{-4}$; n = 19 and 9, control and RNAi animals, respectively).

Combined suppression of low-frequency lineages affects neoblast colony formation

Our model and simulations indicate that inhibition of smaller lineages will not result in detectably smaller colonies (**Fig S3A-C**). We tested this model prediction by comparing colonies produced following suppression of intestine lineage progenitors (Forsthoefel et al., 2012; van Wolfswinkel et al., 2014; Wagner et al., 2011), which account for 14% of the produced progenitors (Raz et al., 2021). Indeed, highly efficient inhibition of the intestine lineage by RNAi (**Fig S3D**), did not result in reduced colony size or colony production, in agreement with our model (**Fig 4G-H**, S3A). This result corroborated the model's predictions regarding lower-frequency lineages (**Fig 3A**): the potential increase in q following suppression of differentiation to a lower-frequency lineage had undetectable effect on colony size. However, the model predicts that inhibition of several lineages, which collectively amount to a larger fraction of produced progenitors, may generate a detectable difference in successful colony establishment. We co-suppressed the production of intestine lineage together with *foxF-1*$^{+}$ progenitors, which together amount to 25% of the progenitors (Raz et al., 2021), following subtotal irradiation (**Fig 4I**). The co-inhibition of the two lineages resulted in a highly significant increase in the failure to establish colonies (8/9; 88.9%), compared to their controls (3/19; 15.8%; Fisher's exact test two-tailed $P = 4\times10^{-4}$).

These results reinforce the hypothesis that FSTF inhibition reduces colony growth (vs. control), primarily through increased neoblast elimination, without compensatory increases in other lineages. The results also suggest that a neoblast that has selected an identity, but that cannot complete proliferation and differentiation, will not be able to adopt any other identity in this experimental timescale. Based on these conclusions, we propose a semi-stochastic model for selecting the outcome of neoblast division, assuming no memory or coordination between cells, that is sufficient for describing neoblast colony growth.

Inhibition of *zfp-1* does not induce overexpression of other lineages in homeostasis

Clonal analysis is a powerful approach for studying neoblast proliferation and progeny production. However, stem cell behavior in homeostasis may differ from that observed in clonal growth. For example, unlike in clonal expansion, the stem cell population size remains unchanged during homeostasis, indicating the differential activity of feedback mechanisms. Moreover, the vastness of the neoblast population in homeostasis allows to examine the ability of neoblasts to respecify their lineage overtime, and to determine if FSTF inhibition results in an increase to cell loss rate.

We examined whether the suppression of a major lineage production has resulted in overproduction of other lineages, a phenomenon that we did not observe in colonies. First, we used two published gene expression datasets from FACS-purified S/G2/M neoblasts in *zfp-1* (RNAi) and control animals collected at various time points (Cheng et al., 2018; van Wolfswinkel et al., 2014) (Methods). We utilized pre-calculated tables of differentially expressed genes in these datasets (Hoffman and Wurtzel, 2023), and annotated the cell types that express them (Fincher et al., 2018). Most downregulated genes with known neoblast lineage enrichment (Fincher et al., 2018) were epidermal (82%, 55/67; **Fig 5A**; Table S1;

Methods). Conversely, upregulated genes following *zfp-1* suppression were primarily associated with protonephridial or neural neoblasts (30/57 and 20/57 genes, respectively; **Fig 5B**; Table S2), consistent with the original data analysis (Cheng et al., 2018). Notable upregulated genes included transcription factors, such as *nkx2-like* (Currie et al., 2016), *hunchback-like* (Reddien et

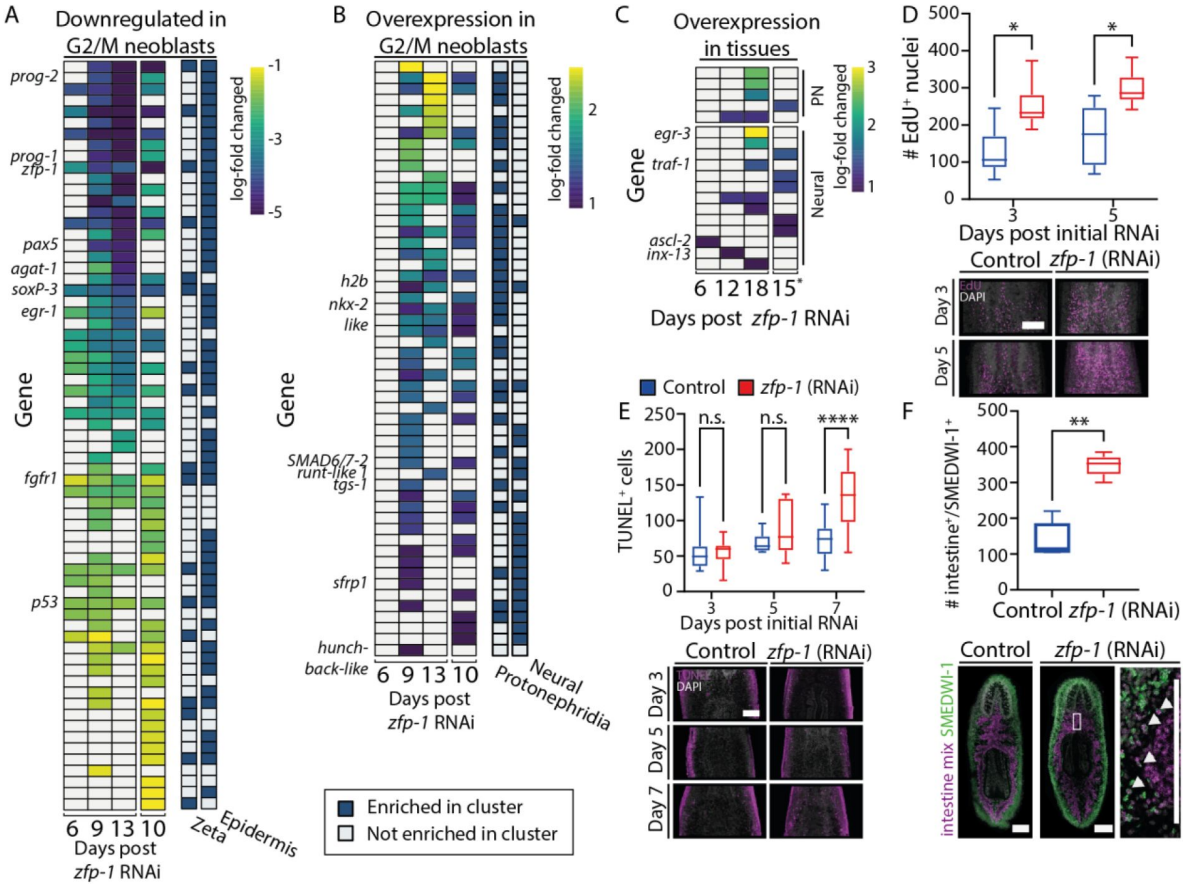

Figure 5.

Analysis of *zfp-1* inhibition consequences in homeostasis.

(A) Downregulated genes in FACS-purified S/G2/M neoblasts were overwhelmingly associated with expression in the epidermal lineage and epidermis-specialized (zeta) neoblasts (Cheng et al., 2018; Fincher et al., 2018; van Wolfswinkel et al., 2014). (B) Upregulated genes in FACS-purified S/G2/M neoblasts were largely associated with neuronal and protonephridial specialized gene expression (Fincher et al., 2018). (C) Analysis of overexpressed genes of whole-tissues following *zfp-1* inhibition showed that only a few factors were associated with protonephridia or neurons. (A-C) Heatmaps showing row-scaled gene expression obtained from PLANAtools (Hoffman and Wurtzel, 2023) Blue and yellow, low and high log-fold gene expression difference, respectively. Columns on the right indicate cell type-specific gene expression (Fincher et al., 2018). (D) Counting EdU$^+$ nuclei in unirradiated control and *zfp-1* (RNAi) animals. (E) Counting apoptotic cells in unirradiated control and *zfp-1* (RNAi) animals (Methods). (F) Counting intestinal progenitors showed an increase in progenitors at later time points, in agreement with the gene expression analysis of *zfp-1* (RNAi) of whole tissues. Scale = 100 μm. * $P < 0.05$; ** $P < 0.01$; **** $P < 0.0001$.

al., 2005a), *runt-1* (Sandmann et al., 2011; Wenemoser et al., 2012), and *tgs-1* (Zeng et al., 2018). Overexpression was evident from an intermediate timepoint (9 days post RNAi), whereas epidermal genes downregulation occurred earlier (6 days post RNAi; 30%, 20/67; FDR < 1E-5).

We hypothesized that biologically meaningful upregulation of neuron- and protonephridia-associated genes in neoblasts following *zfp-1* inhibition would result in overexpression of genes associated with these cell types in whole tissues, reflecting their increased production. To test this hypothesis, we examined published gene expression data from whole and regenerated tissues following *zfp-1* inhibition (van Wolfswinkel et al., 2014; Zeng et al., 2018). Predictably, the majority of downregulated genes were associated with the epidermis (70%, 490/698; Fold change < -2; FDR < 1E-5; Table S3; Methods). Examination of upregulated genes showed that only a small fraction of the genes was associated with either protonephridial (4.9%) or neural (12.7%) expression at any examined time point (**Fig 5C**; Table S4; Methods). Therefore, gene expression analysis of whole tissues provided no evidence of an overrepresentation of neural or protonephridia cells in *zfp-1* (RNAi) animals, suggesting that cells related to these lineages were not excessively produced. Conversely, 37% of the overexpressed genes following *zfp-1* (RNAi) in the whole tissue libraries were associated with intestinal cell types, despite no evidence for overrepresentation of intestine-associated FSTFs in neoblasts isolated from *zfp-1* (RNAi) animals compared to controls (Table S4).

In *zfp-1* (RNAi) neoblast colonies, we observed an absolute reduction in cycling cells (**Fig 3D**). We tested whether this phenotype was recapitulated in homeostatic, unirradiated, *zfp-1* (RNAi) animals by EdU labeling. We injected *zfp-1* or control double-stranded (dsRNA; Methods), and following three and five days, we performed EdU labeling by a 16 hour EdU pulse (Methods). Interestingly, there was an increase in EdU^+ nuclei in the *zfp-1* (RNAi) animals at both timepoints (**Fig 5D**). Investigating the potential correlation with apoptosis via TUNEL labeling revealed no early increase in cell death, only appearing at later stages (**Fig 5E**; Methods). Therefore, *zfp-1* inhibition does not trigger an acute rise in neoblast cell death that might induce hyperproliferation.

Colony sizes following *zfp-1* (RNAi) were reduced, yet cycling cell numbers in homeostasis were increased. Similar results were reported for the epidermal regulator *Smed-p53* (Cheng et al., 2018; Pearson and Sánchez Alvarado, 2010): neoblast colonies following *p53* (RNAi) are strikingly smaller (Wagner et al., 2012), yet in homeostasis, *p53* (RNAi) animals show an increased number of mitoses (Pearson and Sánchez Alvarado, 2010), and even initially an increase in canonical neoblast markers (Pearson and Sánchez Alvarado, 2010).

Considering that in homeostasis *zfp-1* (RNAi) planarians show greater numbers of cycling cells (**Fig 5D**) and intestinal gene overexpression in tissue (Table S4) as compared with controls, we conducted a targeted analysis to quantify the number of newly generated intestine progenitors in *zfp-1* (RNAi) animals. We counted intestine progenitors *in situ* (**Fig 5F**; Methods), and found a higher proportion of intestine progenitors in the *zfp-1* (RNAi) animals as compared with controls (**Fig 5F**; Mann–Whitney two-tailed U test $P = 0.008$). Interestingly, in our analyses of growing colonies, we did not observe a parallel difference in intestine neoblast proportion (**Fig 4A**), leading us to speculate that the rise in cycling cells in homeostasis was an indirect effect of *zfp-1* RNAi suppression, and indicating of the limits of neoblast analysis in colonies. In other words, integration of the analysis from homeostasis with our colony data suggests that *zfp-1* inhibition did not lead to a direct amplification of other lineages, but more likely to an indirect amplification of the intestine lineage.

Discussion

Understanding how stem cell proliferation and lineage choices are regulated is critical for elucidating mechanisms of growth and homeostasis (Chan et al., 2021; Dagan et al., 2022; Ferraro et al., 2010; Lei et al., 2016; Li and Xie, 2005; Morrison and Spradling, 2008; Scimone et al., 2010; Zhu et al., 2015).

Neoblasts form a simple yet powerful system, which has features of both adult stem cells and their transit-amplifying cell progeny (Adler and Sánchez Alvarado, 2015; Baguñà, 2012; Reddien, 2018). Functionally, neoblasts can repopulate stem cell-depleted planarians, produce a diversity of cell types, and adjust their growth rate according to organism requirements and nutrient availability (Hayashi et al., 2006; Salvetti et al., 2009; Steele and Lange, 1976; Wang et al., 2018). Herein, we sought to test whether growth in a neoblast colony is consistent with a model that does not assume communication between neoblasts or memory of cell fate decisions, but instead relies on stochastic selection of division outcome (**Fig 6**). We further sought to enrich this model by understanding the interplay between neoblast lineage decisions and colony growth.

Analysis of neoblast colony expansion

The initial model we developed was grounded in simple principles of colony growth (**Eq 1**, **Fig 2B**), in which cell fate decisions are made stochastically and independently of one another, as a function of the following parameters: average cell cycle length, symmetric renewal rate, and symmetric differentiation and neoblast elimination rate. We experimentally derived parameter values and compared the model's predictions to experimental data. Our findings suggested that the reliance on minimal assumptions provides a good description of neoblast colony growth following subtotal irradiation. The model captured the average colony growth within the tested time range, despite notable variability in observed colony sizes at a given time point. Based on these results, we suggest that if slow cycling neoblasts (Molinaro et al., 2021) emerge in colonies, their contribution for colony growth is likely negligible, allowing their exclusion from the model without sacrificing accuracy.

To better understand the potential consequences of random neoblast loss or excessive symmetric differentiation at early stages of colony growth, we used colony growth simulations, where each cell selected independently the outcome of its division. These simulations predicted that a fraction of colonies would fail to develop because of these random effects, a prediction that was corroborated by experimental results. This alignment demonstrates the utility of neoblasts as a system for studying stem cell colony formation and exploring concepts of stem cell behavior.

Consequences of lineage-specific differentiation inhibition

Moving from the fundamental aspects of neoblast colony growth, we next tested how limiting lineage identity selection affected neoblasts. We suppressed the expression of key fate-specifying genes to dissect how stem cells respond to inhibition of their differentiation trajectory. The transition from measuring general colony growth to specific lineage perturbations allowed us to examine the association of proliferation and lineage specification. In particular, suppressing the master epidermal regulator *zfp-1*, corresponding to the most abundant planarian cell lineage (Cheng et al., 2018; Raz et al., 2021; van Wolfswinkel et al., 2014), drastically reduced neoblast colony growth. This observation led us to consider how stem cells in a colony balance self-renewal and differentiation, and why both processes were disrupted by blocking differentiation to a single lineage. We suggest several interpretations for this observation: First, if we assume that a neoblast can alternate between self-renewal and production of differentiated progeny in each cell cycle, then a decision to produce a blocked progeny may preclude further

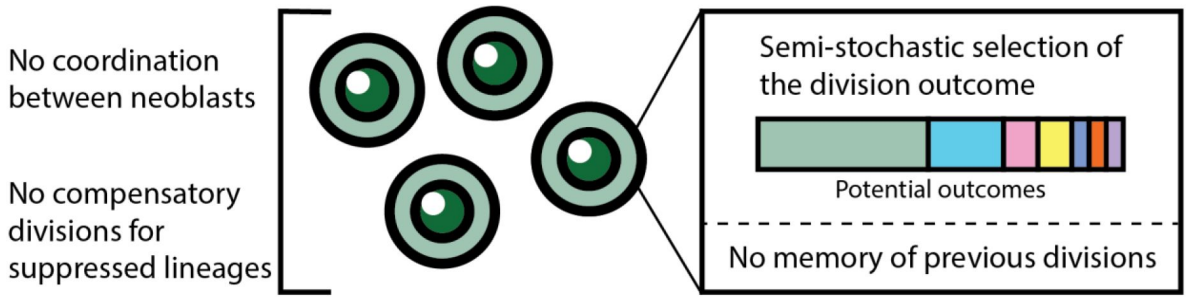

Figure 6.

Model summarizing neoblast colony growth principles.

divisions of the neoblast. A second possibility is that the presence of a specific lineage, epidermal progenitors in this case, is required for other neoblasts to proliferate; in this case, suppression of differentiation could indirectly limit colony growth. The first interpretation is more likely relevant for understanding colony growth given our observation that combined suppression of several smaller lineages produced a similar inhibition to colony establishment.

The progressive reduction in colony size indicated that inhibition of a specific lineage reduced the fraction of neoblasts that contributed to colony growth, possibly due to their failure to produce the blocked lineage and to alter their progeny identity. Interestingly, in unirradiated animals with abundant neoblasts, *zfp-1* inhibition led to increased cell proliferation – a response also noted after suppressing other regulatory genes like *Smed-p53* (Pearson and Sánchez Alvarado, 2010). This proliferation increase appeared before a rise in cell death, suggesting that cell death did not induce excessive proliferation in early stages. The difference in the consequence of lineage suppression in a neoblast colony and in unirradiated animals indicates that differential activity of feedback mechanisms regulates neoblast proliferation. We speculate that following subtotal irradiation, the near complete depletion of neoblasts and their progeny (Eisenhoffer et al., 2008), alters the regulation of surviving neoblasts, and leading to their rapid proliferation, which is not typical for neoblasts in homeostasis (Wenemoser and Reddien, 2010). Further investigation is needed into compensatory mechanisms that planarians use to maintain overall tissue integrity when differentiation processes are disrupted.

A stochastic model for independent selection of cell division outcome in colonies

Our study investigates the mechanism behind neoblast division outcome selection. An exponential growth function describes the increase in colony size and the differentiation of progeny in the timescale of the analysis, closely aligning with our experimental results and published data (Raz et al., 2021; Wagner et al., 2012). Notably, this function operates without parameters for coordination of division outcome between neoblasts, or neoblast memory. It posits that division outcomes are guided by an innate distribution of cell fates encoded within the neoblasts. We hypothesize that this distribution is modifiable by regional signals (e.g., Wnt, BMP), which indicate the neoblast location (Gaviño and Reddien, 2011; Petersen and Reddien, 2008; Wurtzel et al., 2017), and by injury signals (e.g., ERK), that modulate division rate (Bohr et al., 2021; Fan et al., 2023; Tasaki et al., 2011; Wurtzel et al., 2015). This strategy facilitates the dynamic balance in cell lineage production and meeting the organism needs without direct communication between neoblasts, and promotes return to homeostasis.

The emerging model enhances the understanding of neoblast dynamics and contributes to broader knowledge of stem cell behavior. The interplay between lineage-specific differentiation, proliferation, and resultant physiological adaptations presents a robust strategy for using pluripotent stem cells for re-achieving balance, in a manner that is not found in many non-regenerative organisms. This could inspire future research of pluripotent stem cells and their applications for regenerative biology.

Methods

Gene cloning and transformation

Selected genes were amplified using planarian cDNA and gene-specific primers, and cloned into pGEM-T Easy vector using pGEM-T Easy Vector System I (Promega; CAT A1360). Vectors were transformed into *Escherichia coli* using the heat-shock method. Briefly, 5 µl of cloned plasmid were mixed with 100 µl of *E. coli* TOP10 bacteria and incubated on ice for 30 min. Next, bacteria were incubated for 45 s at 42°C, moved immediately to ice, and recovered in 350 µl of Luria Broth (LB)

medium for 1 h at 37°C. Then, 100 µl of recovered bacteria were plated on agarose plates containing 1:1,000 Ampicillin, 1:200 Isopropyl β-d-1-thiogalactopyranoside (IPTG) and 1:625 5-bromo-4-chloro-3-indolyl-b-D-galactopyranoside (X-Gal). Plates were incubated overnight at 37°C, and colonies were screened by colony PCR using M13F and M13R primers with the following PCR program: (i) 5 min at 95°C; (ii) 34 cycles of 45 s at 95°C, 60 s at 55°C, and 2 min at 72°C; (iii) 7 min at 72°C; (iv) hold at 10°C. Reactions were analyzed by gel electrophoresis, and colonies having the correct fragment were grown overnight in LB medium, supplemented with 1:1,000 Ampicillin at 37°C in 180 rpm. Plasmids were purified with the NucleoSpin Plasmid MiniprepKit (CAT 740588, Macherey-Nagel) and sequenced by Sanger sequencing. Primer sequences used for cloning the following genes: *hnf-4*, forward primer GATCTCGCACAATGCACTCG, reverse primer GTCTCACGAACTCCTTGCCA; *nkx2.2*, forward primer TTTGGTGCCAGCAGACTCAA, reverse primer TAGAGCCAGCTAATGTGGCG; *gata4/5/6*, forward primer CGGTATTGTCGAATTCTCACCAG, reverse primer TGACATCGCAATTGGAACCG; *foxF-1*, forward primer GTCCTATTTCCAGCACACAGC, reverse primer TCCGGAATCGTGCTGAGG.

Near complete neoblast ablation by subtotal irradiation

Animals were irradiated using a BIOBEAM GM 8000 (Gamma-Service Medical GmbH). To generate 1-3 colonies per animal, 2 mm starved (> 7 d) worms were irradiated with 1750 rads (Wagner et al., 2012). Worms were allowed to recover and washed in planarian water a day after the irradiation.

Synthesis of dsRNA for feedings and microinjections

DsRNA was synthesized as previously described (Rouhana et al., 2013). Briefly, templates for in vitro transcription (IVT) were prepared by PCR amplification of cloned target genes using forward and reverse primers with flanking T7 promoter sequences on the 5' end. dsRNA was synthesized using the TranscriptAid T7 High Yield Transcription Kit (CAT K0441, Thermo Scientific). Reactions were incubated overnight at 37°C and then supplemented with RNase-free DNase for 30 min. RNA was purified by ethanol precipitation and resuspended in 70 µl of ultra-pure H2O. RNA was analyzed on 1% agarose gel and quantified by Qubit (CAT Q33223, Thermo Scientific) for validating a concentration higher than 5 µg/µl. Animals were starved for at least 7 d prior to RNAi experiments. In clonal expansion experiments, animals were fed with 14 µl of dsRNA mixed with 25 µl of beef liver 4 days post-irradiation. In homeostasis experiments, worms were injected 4 times with dsRNA every other day.

Injections of dsRNA into planarians

Animals were injected with *zfp-1* dsRNA using Nanoject III (CAT 3-000-207, Drummond Scientific company). Briefly, planarians were placed on a cold wet filter paper on their dorsal side, and were injected posterior to the pharyngeal cavity. After the initial puncture, 3 consecutive dsRNA injections of 33 nl each were delivered at a rate of 66 nl/sec. Worms were injected 4 times, every other day, and fixed at different time points for whole-mount analysis.

Planarian fixation for whole-mount assays

Fixation was performed as previously described (King and Newmark, 2013). Animals were killed with 5% N-Acetyl-L-Cysteine (NAC, CAT 1124220100, Mercury) in PBS for 5 min, then incubated with 4% Formaldehyde (FA) in 0.3% PBSTx (Phosphate Buffered Saline, 0.3% Triton X-100) for 20 min. Animals were then washed in PBSTx, 50:50 PBSTx:methanol and stored in methanol at -20°C.

Fluorescence in situ hybridization using tyramide signal amplification

Fluorescence in situ hybridization (FISH) was performed as previously described (King and Newmark, 2013) with minor changes. Briefly, fixed animals were bleached and treated with proteinase K (2 µg/ml, CAT 25530-049; Invitrogen) in PBSTx (Phosphate Buffered Saline, 0.3% Triton X-100). Samples were incubated for 2 hr in a pre-hybridization buffer (pre-hyb) followed by an overnight incubation with probes. Samples were washed twice for 30 min in each solution: pre-hyb solution, 1:1 pre-hyb:2×SSCx, 2×SSCx, 0.2×SSCx, PBSTx. Blocking was performed in 0.5% Roche Western Blocking Reagent (CAT 11921673001; Sigma-Aldrich) and 5% heat-inactivated horse serum (CAT 04-124-1A; Biological Industries) in TNTx (100 mM Tris pH 7.5, 150 mM NaCl, 0.3% Triton X-100) for 2 hr. Animals were incubated with an anti-DIG-POD antibody (1:1,500; Roche) or anti-DNP-HRP (1:10,000; Perkin-Elmer) overnight at 4°C. After antibody washes, tyramide development was performed as previously described (King and Newmark, 2018). Following development, peroxidase activation was quenched in a 1% sodium azide solution for 1 hr, followed by 6 PBSTx washes and antibody labeling for the second probe. Samples were labeled with DAPI (1:5000 in PBSTx) overnight at 4°C and mounted with Vectashield (CAT H-1000-10; Vector Laboratories).

Immunofluorescence combined with FISH

Animals were fixed with 5% NAC, bleached, and treated with proteinase K as described for FISH analysis. Samples were incubated for 2 hr in pre-hyb followed by overnight incubation with the probes. Samples were washed twice in each solution, for 30 min each: pre-hyb solution, 1:1 pre-hyb:2×SSCx, 2×SSCx, 0.2×SSCx, PBSTx. Subsequently, blocking was performed in PBSTB (PBSTx, 0.25% BSA) for 2 hr at room temperature. Animals were then incubated with anti-SMEDWI-1 antibody (a gift from Peter W. Reddien, 1:1000) at 4°C overnight. Then, 7 PBSTx washes were performed, followed by incubation with PBSTB blocking solution for 2 hr at room temperature followed by incubation with secondary antibody (goat anti rabbit-HRP, 1:300 in PBSTB) overnight at 4°C. Post-antibody washes and tyramide development (fluorescein tyramide; 1:2000) were performed as previously described (King and Newmark, 2013). After development, peroxidase activity was quenched using 1% sodium azide for 1 hr, followed by 6 PBSTx washes and incubation with anti-DIG antibody (1:1,500; CAT 11207733910; Sigma-Aldrich) overnight at 4°C. Post-antibody washes and development with rhodamine tyramide (1:1000) were performed as described above. Samples were incubated with DAPI (1:5000 in PBSTx) overnight and mounted with Vectashield.

FISH by hybridization chain reaction

Probe sets (30 pairs per gene) were designed and synthesized by the manufacturer (Molecular Instruments, Los Angeles, CA, USA) for the following genes: *tgs-1* and *smedwi-1*. Worms were fixed and bleached as previously described for FISH. Next, hybridization chain reaction (HCR) was performed according to the manufacturer's HCR RNA-FISH protocol for samples in solution (Choi et al., 2018). DAPI was added during the amplifier's wash steps, for a total incubation time of 2 hr at room temperature. Samples were mounted with Vectashield and stored at 4°C for subsequent analysis.

Metabolic labeling by F-ara-EdU

F-ara-EdU (CAT T511293; Sigma-Aldrich) was first diluted in DMSO to the concentration of 200 mg/ml. Animals were soaked with 2.5 mg/ml F-ara-EdU diluted in planarian water for 16 hr, 24 hr after the indicated injections. For clonal expansion analysis, samples were soaked with EdU for 16 hr at day 11 post irradiation. Samples were fixed, bleached, and treated with proteinase K as described for FISH (King and Newmark, 2013). Next, 3 washes in 3% PBSB (PBS supplemented

with 3% BSA) were performed followed by a click reaction using baseclick kit (CAT Back-edu488, baseclick GmbH). Samples were washed 3 times with PBSB, incubated with DAPI (1:5,000 in PBSTx) overnight at 4°C and mounted with Vectashield.

Immunofluorescence labeling by anti-H3P labeling

H3P labeling was performed as previously described (LoCascio et al., 2017; Wenemoser and Reddien, 2010) with minor modifications. Briefly, following fixation with 5% NAC, bleaching and proteinase K treatment, blocking was performed with 10% heat inactivated horse serum for 2 hr. Next, anti-phospho-Histone H3 Antibody (CAT 04817; Sigma-Aldrich) was added in the concentration of 1:100 overnight in 4°C, followed by 7 PBSTx washes. Samples were incubated in blocking solution for 2 hr and then incubated with goat anti-rabbit-HRP secondary antibody (Abcam; ab6721; 1:300) overnight at 4°C. Samples were washed 7 times with PBSTx, developed using rhodamine tyramide diluted 1:1,000 in PBSTi (PBSTx, 0.07% imidazole), labeled with DAPI overnight at 4°C, and mounted with Vectashield.

Image acquisition and cell counting

Images of samples labeled by FISH, HCR, immunofluorescence, F-ara-EdU and TUNEL were collected using a Zeiss LSM800 confocal microscope. Labeled cells were counted manually using the cell counter module in the ImageJ software (Rueden et al., 2017). Normalization of EdU^+ nuclei was performed by dividing the number of EdU^+ nuclei by the average number of *smedwi-1*$^+$ cells detected in a colony at the corresponding time point, and divided by 10 for readability.

TUNEL labeling

TUNEL was performed as previously described (Pellettieri, 2010) with minor modifications. Briefly, animals were fixed with 5% NAC and bleached overnight with 6% hydrogen peroxide in PBSTx. Animals were then treated with 2 µg/ml proteinase K for 10 min, 4% FA for 10 min, and were then washed twice with PBS. Using ApopTag Red In Situ Apoptosis Detection Kit (CAT S7165; Sigma-Aldrich), 5 animals per tube were incubated with TdT enzyme mix for 4 hr at 37°C, followed by 4 PBSTx washes. Samples were incubated in a blocking solution (0.5% Roche Western Blocking Reagent and 5% inactivated horse serum in TNTx) for 2 hr followed by incubation with anti-DIG antibody (1:1000) overnight at 4°C. Samples were washed 7 times with PBSTx, developed using rhodamine tyramide diluted 1:1,000, labeled with DAPI (1:5000 in PBSTx) overnight at 4°C and mounted with Vectashield.

Estimation of the fraction of symmetric renewal divisions

Estimation of the fraction of symmetric renewal divisions was performed as previously described (Lei et al., 2016; Raz et al., 2021). Colonies from 7, 9, and 12 dpi were labeled by FISH with the pan-neoblast marker *smedwi-1*. Colonies were closely examined using a confocal microscope (Zeiss LSM800) to find two adjacent *smedwi-1*+ cells. Two labeled cells with high expression of *smedwi-1* marker were classified as symmetric division. Pairs composed of high *smedwi-1*+ cell and low *smedwi-1*+ cell were classified as asymmetrically dividing.

Data extraction from published literature

Data was extracted using WebPlotDigitizer by labeling data points (Drevon et al., 2017). Table S5 summarizes the extracted data and the original data source.

Estimation of values of colony growth parameters

Counts of neoblast in colonies at different time points following subtotal irradiation (**Fig 2F**, Table S5) were collected. Curve fitting using an exponential function (**Eq 2**) was performed with the curve_fit function from the scipy.optimize Python module using the average cell cycle length (τ) extracted from the $BrdU^+$ labeling assay (**Fig 2C**; S1B-E) (Lei et al., 2016). The values of

symmetric renewal (p) and symmetric differentiation or elimination (q) were estimated by fitting a range of values for $p - q$ between 0.1 and 0.4 and calculating the R-squared values of the fit to the data (S1D-E). Experimental assessment of symmetric renewal (p) and asymmetric division (a) determined that they are equal (i.e., $p = a$; **Fig 2D**). The best fit, as estimated by examining the sum square of residuals (**Fig S1B-E**), for $p - q$ was found to be 0.3445. Since (1) all possible division outcomes are $p + q + a = 1$; (2) $p = a$; and (3) $p - q = 0.3445$, we estimated that $p = 0.45$ and $q = 0.1$.

Simulation of colony growth

Simulations were performed using custom R code, executing as follows: selection of parameters occurred using selected frequencies of symmetric renewal, and symmetric differentiation or elimination. Initial colony size was determined by randomly selecting a value from empirical distribution of early colony size, as reported in the literature (Raz et al., 2021; Wagner et al., 2011). In each simulation round, every cell underwent selection of an outcome, adhering to the predefined frequencies. This simulation process extended 5 – 20 cycles and was replicated 100 times.

Gene expression analysis of S/G2/M neoblasts

Processed differential gene expression data profiling FACS-purified S/G2/M neoblasts isolated from control and *zfp-1* (RNAi) animals was downloaded from PLANATools (Hoffman and Wurtzel, 2023). Each gene in the table was assigned a cell type identity based on the planarian cell type gene expression atlas (Fincher et al., 2018).

Statistical analyses

Statistical tests were performed using GraphPad Prism (v 10.0.3), using the scipy stat module (v 1.12), and R (v 4.3.2). Statistical significance was assessed using Mann-Whitney two-tailed U test or two-tailed Student's t test and threshold for considering an effect significant was 0.05, unless stated otherwise.

Supplementary Figures

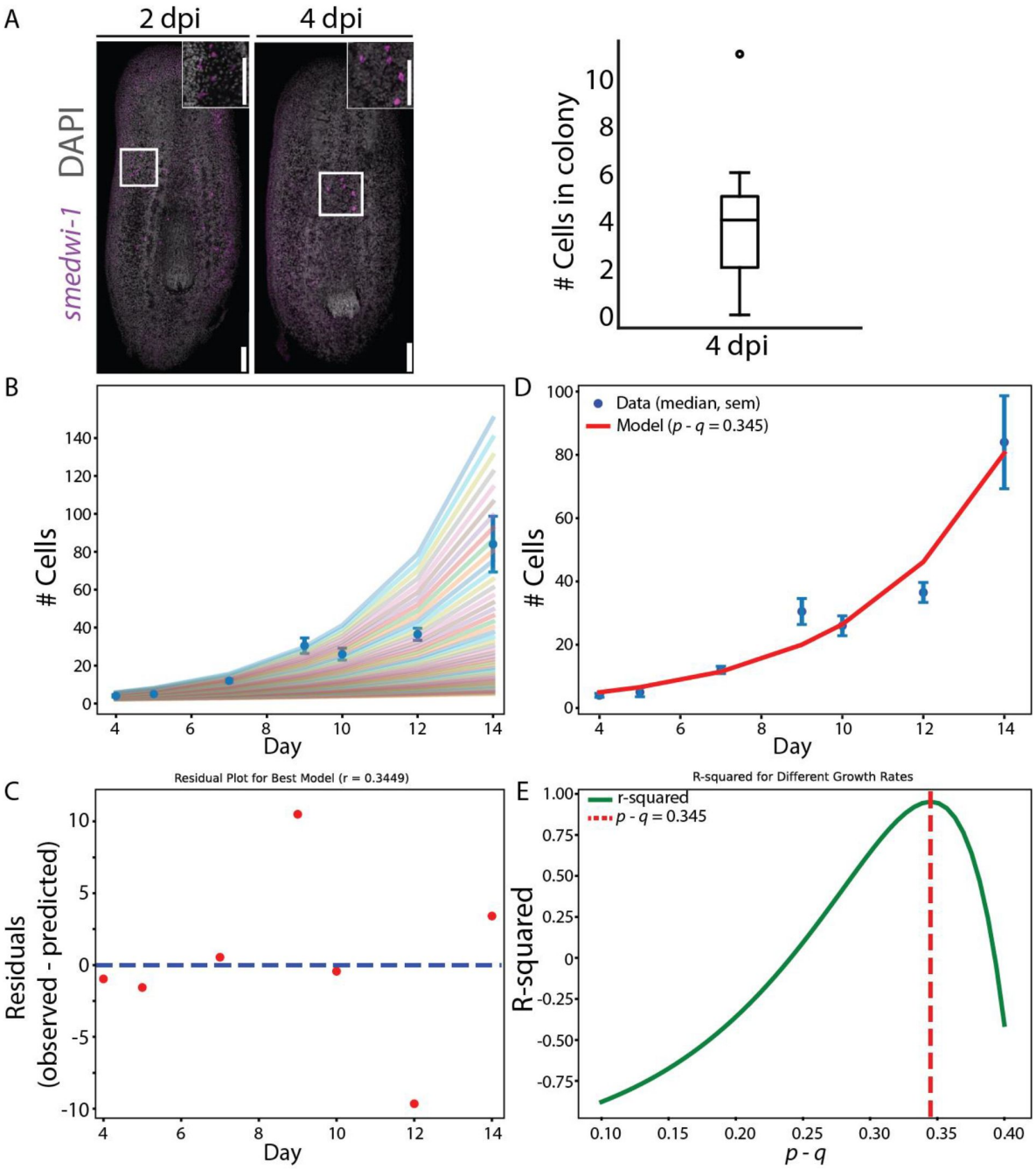

Figure S1.

Analysis of colony growth.

(A) Shown are FISH images for detecting neoblasts (*smedwi-1*$^{+}$; magenta) at 2 and 4 days post irradiation (dpi), left and right, respectively. Colonies were not found at 2 dpi, and instead isolated *smedwi-1*+ were scattered in the planarian parenchyma. At 4 dpi, single neoblasts already established small colonies (median = 4 cells; quantification shown on right). (B-E) The effect of different growth parameters on colony size. (B) Shown are colony sizes when considering a range of *q* values (0.1 - 0.4) with the experimentally determined *p* = 0.5. Data collected here and in published analyses of colony sizes (Raz et al., 2021; Wagner et al., 2012) is shown as median (blue dots, and standard error of the mean). (C) Shown is the best predicted fit growth following colony establishment using the exponential growth equation. (D) Analysis of residuals between observed and predicted colony sizes using the best fitting parameters. (E) Shown is the r-squared difference between observed and predicted data at a range of growth parameters. The minimal r-squared value is indicated by the red dashed line.

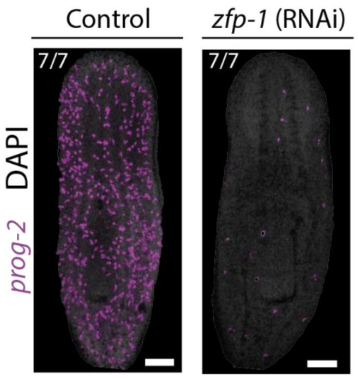

Figure S2.

Inhibition of epidermal progenitors by a single *zfp-1* dsRNA injection.

Inhibition of *zfp-1* resulted in complete ablation of epidermal progenitor production as observed by labeling animals with the epidermal progenitor marker, *prog-2*.

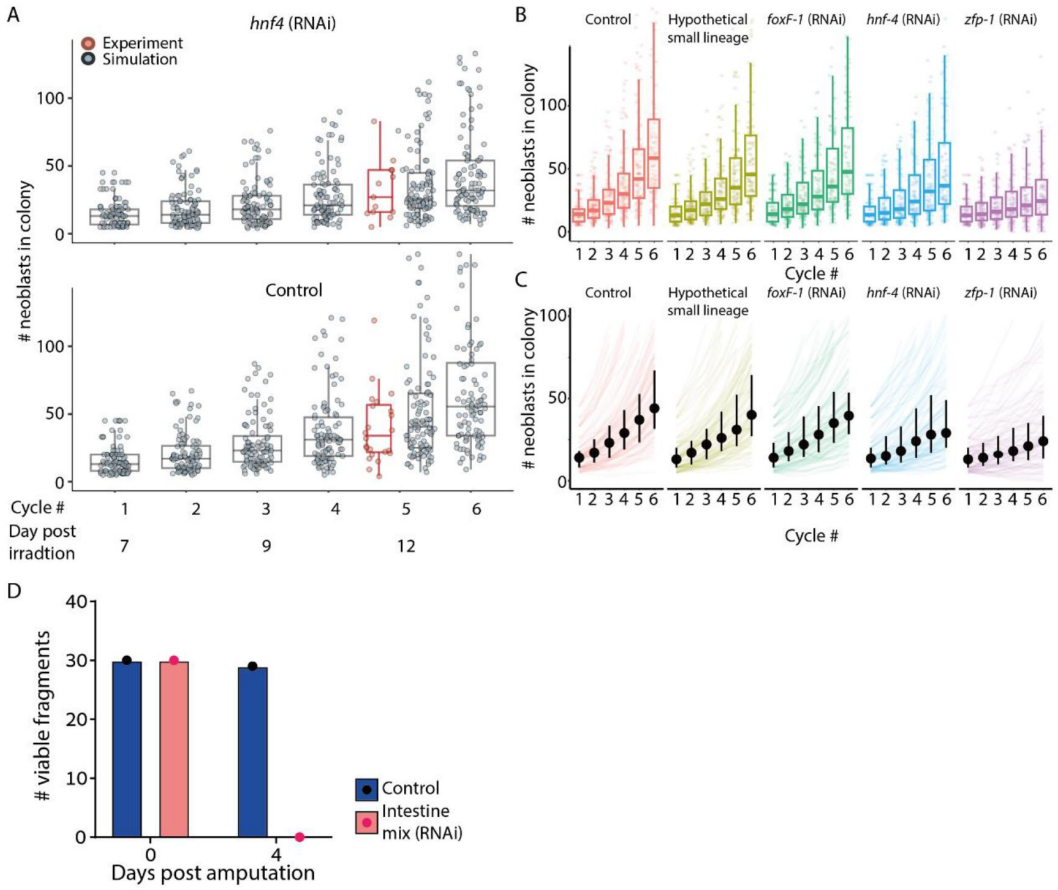

Figure S3.

Simulation of colony size following RNAi.

(A) Simulation (gray) and comparison to experimental data (red) of neoblast colonies in control and *hnf-4* (RNAi) animals. The simulation indicates that given the variability in colony size, detecting significant differences in colony size is unlikely for this lineage. Each dot represents a single simulation (gray) or an experimentally determined size (red). (B-C) Simulations of colony sizes over 6 cycles of replication starting approximately at day seven post irradiation. (B) Boxplots showing the distribution of colony sizes (horizontal line, median; box, interquartile range (IQR); vertical line, 99% range). Each dot represents a single simulation. (C) Simulation of colony growth (line) shows growth over time (dot, median; vertical line, IQR). (D) The RNAi efficacy was evaluated through assessment of viability of fragments obtained from animals following a single feeding of dsRNA that targeted intestine FSTFs (*hnf-4, gata4/5/6, nkx2.2*), compared to a non-targeting control dsRNA (*unc22*). All fragments derived from worms fed with dsRNA targeting intestine FSTFs died within four days post-feeding, demonstrating that a single dsRNA feeding induced a robust effect.

Author contributions

T.F. and O.W. designed the project. T.F. performed all experiments with support from P.V.C, Y.Y., and S.D.. T.F. performed microscopy and imaging analysis. O.W. performed simulations and RNAseq data analysis. T.F. and O.W. wrote and edited the manuscript.

Declaration of Interests

The authors declare no competing interests.

Acknowledgements

We thank Prof. David Sprinzak, Prof. Iftach Nachman, and Dr. Yasmine Meroz for their critical input. We thank Shrey Jain for his assistance with performing FISH. We thank members of the Wurtzel lab for feedback and discussions. We thank Dr. Daria Makarovsky from the interdepartmental services at Tel Aviv University's Faculty of Medicine for assistance with gamma irradiation. O.W. is supported by the Israel

Science Foundation (grant 2039/18) and the European Research Council (no. 853640). O.W. is a Zuckerman Faculty Scholar.

References

Abkowitz JL, Golinelli D, Harrison DE, Guttorp P (2000) **In vivo kinetics of murine hemopoietic stem cells** *Blood* **96**:3399–3405 https://doi.org/10.1182/blood.V96.10.3399

Adler CE, Sánchez Alvarado A (2015) **Types or states? cellular dynamics and regenerative potential** *Trends Cell Biol* **25**:687–696 https://doi.org/10.1016/j.tcb.2015.07.008

Baguñà J (2012) **The planarian neoblast: the rambling history of its origin and some current black boxes** *Int J Dev Biol* **56**:19–37 https://doi.org/10.1387/ijdb.113463jb

Becker KA, Ghule PN, Therrien JA, Lian JB, Stein JL, van Wijnen AJ, Stein GS (2006) **Self-renewal of human embryonic stem cells is supported by a shortened G1 cell cycle phase** *J Cell Physiol* **209**:883–893 https://doi.org/10.1002/jcp.20776

Bohr TE, Shiroor DA, Adler CE (2021) **Planarian stem cells sense the identity of the missing pharynx to launch its targeted regeneration** *eLife* **10** https://doi.org/10.7554/eLife.68830

Chan A, Ma S, Pearson BJ, Chan D (2021) **Collagen IV differentially regulates planarian stem cell potency and lineage progression** *Proc Natl Acad Sci USA* **118** https://doi.org/10.1073/pnas.2021251118

Cheng L-C, Tu KC, Seidel CW, Robb SMC, Guo F, Sánchez Alvarado A (2018) **Cellular, ultrastructural and molecular analyses of epidermal cell development in the planarian Schmidtea mediterranea** *Dev Biol* **433**:357–373 https://doi.org/10.1016/j.ydbio.2017.08.030

Choi HMT, Schwarzkopf M, Fornace ME, Acharya A, Artavanis G, Stegmaier J, Cunha A, Pierce NA (2018) **Third-generation in situ hybridization chain reaction: multiplexed, quantitative, sensitive, versatile, robust** *Development* **145** https://doi.org/10.1242/dev.165753

Currie KW, Molinaro AM, Pearson BJ (2016) **Neuronal sources of hedgehog modulate neurogenesis in the adult planarian brain** *eLife* **5** https://doi.org/10.7554/eLife.19735

Dagan Y, Yesharim Y, Bonneau AR, Frankovits T, Schwartz S, Reddien PW, Wurtzel O (2022) **m6A is required for resolving progenitor identity during planarian stem cell differentiation** *EMBO J* **41** https://doi.org/10.15252/embj.2021109895

Drevon D, Fursa SR, Malcolm AL (2017) **Intercoder reliability and validity of webplotdigitizer in extracting graphed data** *Behav Modif* **41**:323–339 https://doi.org/10.1177/0145445516673998

Eisenhoffer GT, Kang H, Sánchez Alvarado A (2008) **Molecular analysis of stem cells and their descendants during cell turnover and regeneration in the planarian Schmidtea mediterranea** *Cell Stem Cell* **3**:327–339 https://doi.org/10.1016/j.stem.2008.07.002

Fan Y, Chai C, Li P, Zou X, Ferrell JE, Wang B (2023) **Ultrafast distant wound response is essential for whole-body regeneration** *Cell* **186**:3606–3618 https://doi.org/10.1016/j.cell.2023.06.019

Ferraro F, Celso CL, Scadden D (2010) **Adult stem cells and their niches** *Adv Exp Med Biol* **695**:155–168 https://doi.org/10.1007/978-1-4419-7037-4_11

Fincher CT, Wurtzel O, de Hoog T, Kravarik KM, Reddien PW (2018) **Cell type transcriptome atlas for the planarian Schmidtea mediterranea** *Science* **360** https://doi.org/10.1126/science.aaq1736

Forsthoefel DJ, James NP, Escobar DJ, Stary JM, Vieira AP, Waters FA, Newmark PA (2012) **An RNAi screen reveals intestinal regulators of branching morphogenesis, differentiation, and stem cell proliferation in planarians** *Dev Cell* **23**:691–704 https://doi.org/10.1016/j.devcel.2012.09.008

Gaviño MA, Reddien PW (2011) **A Bmp/Admp regulatory circuit controls maintenance and regeneration of dorsal-ventral polarity in planarians** *Curr Biol* **21**:294–299 https://doi.org/10.1016/j.cub.2011.01.017

González-Estévez C, Felix DA, Rodríguez-Esteban G, Aboobaker AA (2012) **Decreased neoblast progeny and increased cell death during starvation-induced planarian degrowth** *Int J Dev Biol* **56**:83–91 https://doi.org/10.1387/ijdb.113452cg

Hayashi T, Asami M, Higuchi S, Shibata N, Agata K (2006) **Isolation of planarian X-ray-sensitive stem cells by fluorescence-activated cell sorting** *Dev Growth Differ* **48**:371–380 https://doi.org/10.1111/j.1440-169X.2006.00876.x

Hoffman M, Wurtzel O (2023) **PLANAtools-An interactive gene expression repository for the planarian Schmidtea mediterranea** *Front Cell Dev Biol* **11** https://doi.org/10.3389/fcell.2023.1149537

King RS, Newmark PA (2018) **Whole-Mount In Situ Hybridization of Planarians** *Methods Mol Biol* **1774**:379–392 https://doi.org/10.1007/978-1-4939-7802-1_12

King RS, Newmark PA (2013) **In situ hybridization protocol for enhanced detection of gene expression in the planarian Schmidtea mediterranea** *BMC Dev Biol* **13** https://doi.org/10.1186/1471-213X-13-8

Lei K, Thi-Kim Vu H, Mohan RD, McKinney SA, Seidel CW, Alexander R, Gotting K, Workman JL, Sánchez Alvarado A (2016) **Egf signaling directs neoblast repopulation by regulating asymmetric cell division in planarians** *Dev Cell* **38**:413–429 https://doi.org/10.1016/j.devcel.2016.07.012

Levin M, Pietak AM, Bischof J (2019) **Planarian regeneration as a model of anatomical homeostasis: Recent progress in biophysical and computational approaches** *Semin Cell Dev Biol* **87**:125–144 https://doi.org/10.1016/j.semcdb.2018.04.003

Li L, Xie T (2005) **Stem cell niche: structure and function** *Annu Rev Cell Dev Biol* **21**:605–631 https://doi.org/10.1146/annurev.cellbio.21.012704.131525

LoCascio SA, Lapan SW, Reddien PW (2017) **Eye Absence Does Not Regulate Planarian Stem Cells during Eye Regeneration** *Dev Cell* **40**:381–391 https://doi.org/10.1016/j.devcel.2017.02.002

Mangel M, Bonsall MB, Aboobaker A (2016) **Feedback control in planarian stem cell systems** *BMC Syst Biol* **10** https://doi.org/10.1186/s12918-016-0261-8

Molinaro AM, Lindsay-Mosher N, Pearson BJ (2021) **Identification of TOR-responsive slow-cycling neoblasts in planarians** *EMBO Rep* **22** https://doi.org/10.15252/embr.202050292

Morrison SJ, Spradling AC (2008) **Stem cells and niches: mechanisms that promote stem cell maintenance throughout life** *Cell* **132**:598–611 https://doi.org/10.1016/j.cell.2008.01.038

Passegué E, Jamieson CHM, Ailles LE, Weissman IL (2003) **Normal and leukemic hematopoiesis: are leukemias a stem cell disorder or a reacquisition of stem cell characteristics?** *Proc Natl Acad Sci USA* **100**:11842–11849 https://doi.org/10.1073/pnas.2034201100

Pearson BJ, Sánchez Alvarado A (2010) **A planarian p53 homolog regulates proliferation and self-renewal in adult stem cell lineages** *Development* **137**:213–221 https://doi.org/10.1242/dev.044297

Pearson BJ (2022) **Finding the potency in planarians** *Commun Biol* **5** https://doi.org/10.1038/s42003-022-03905-9

Pellettieri J (2010) **Cell death and tissue remodeling in planarian regeneration** *Dev Biol*

Petersen CP, Reddien PW (2008) **Smed-betacatenin-1 is required for anteroposterior blastema polarity in planarian regeneration** *Science* **319**:327–330 https://doi.org/10.1126/science.1149943

Raz AA, Wurtzel O, Reddien PW (2021) **Planarian stem cells specify fate yet retain potency during the cell cycle** *Cell Stem Cell* **28**:1307–1322 https://doi.org/10.1016/j.stem.2021.03.021

Reddien PW, Bermange AL, Murfitt KJ, Jennings JR, Sánchez Alvarado A (2005) **Identification of genes needed for regeneration, stem cell function, and tissue homeostasis by systematic gene perturbation in planaria** *Dev Cell* **8**:635–649 https://doi.org/10.1016/j.devcel.2005.02.014

Reddien PW, Oviedo NJ, Jennings JR, Jenkin JC, Sánchez Alvarado A (2005) **SMEDWI-2 is a PIWI-like protein that regulates planarian stem cells** *Science* **310**:1327–1330 https://doi.org/10.1126/science.1116110

Reddien PW (2018) **The cellular and molecular basis for planarian regeneration** *Cell* **175**:327–345 https://doi.org/10.1016/j.cell.2018.09.021

Reddien PW (2013) **Specialized progenitors and regeneration** *Development* **140**:951–957 https://doi.org/10.1242/dev.080499

Rouhana L, Weiss JA, Forsthoefel DJ, Lee H, King RS, Inoue T, Shibata N, Agata K, Newmark PA (2013) **RNA interference by feeding in vitro-synthesized double-stranded RNA to planarians: methodology and dynamics** *Dev Dyn* **242**:718–730 https://doi.org/10.1002/dvdy.23950

Rueden CT, Schindelin J, Hiner MC, DeZonia BE, Walter AE, Arena ET, Eliceiri KW (2017) **ImageJ2: ImageJ for the next generation of scientific image data** *BMC Bioinformatics* **18** https://doi.org/10.1186/s12859-017-1934-z

Salvetti A, Rossi L, Bonuccelli L, Lena A, Pugliesi C, Rainaldi G, Evangelista M, Gremigni V (2009) **Adult stem cell plasticity: neoblast repopulation in non-lethally irradiated planarians** *Dev Biol* **328**:305–314 https://doi.org/10.1016/j.ydbio.2009.01.029

Sandmann T, Vogg MC, Owlarn S, Boutros M, Bartscherer K (2011) **The head-regeneration transcriptome of the planarian Schmidtea mediterranea** *Genome Biol* **12** https://doi.org/10.1186/gb-2011-12-8-r76

Scimone ML, Kravarik KM, Lapan SW, Reddien PW (2014) **Neoblast specialization in regeneration of the planarian Schmidtea mediterranea** *Stem Cell Reports* **3**:339–352 https://doi.org/10.1016/j.stemcr.2014.06.001

Scimone ML, Meisel J, Reddien PW (2010) **The Mi-2-like Smed-CHD4 gene is required for stem cell differentiation in the planarian Schmidtea mediterranea** *Development* **137**:1231–1241 https://doi.org/10.1242/dev.042051

Scimone ML, Wurtzel O, Malecek K, Fincher CT, Oderberg IM, Kravarik KM, Reddien PW (2018) **foxF-1 Controls Specification of Non-body Wall Muscle and Phagocytic Cells in Planarians** *Curr Biol* **28**:3787–3801 https://doi.org/10.1016/j.cub.2018.10.030

Singh SR, Burnicka-Turek O, Chauhan C, Hou SX (2011) **Spermatogonial stem cells, infertility and testicular cancer** *J Cell Mol Med* **15**:468–483 https://doi.org/10.1111/j.1582-4934.2010.01242.x

Steele VE, Lange CS (1976) **Effects of irradiation on stem cell response to differentiation inhibitors in the planarian Dugesia etrusca** *Radiat Res* **67**:21–29

Tasaki J *et al.* (2011) **ERK signaling controls blastema cell differentiation during planarian regeneration** *Development* **138**:2417–2427 https://doi.org/10.1242/dev.060764

Tu KC, Cheng L-C, Vu H T K, Lange JJ, McKinney SA, Seidel CW, Sánchez Alvarado A (2015) **Egr-5 is a post-mitotic regulator of planarian epidermal differentiation** *eLife* **4** https://doi.org/10.7554/eLife.10501

Van Roten A, Barakat AZA-Z, Wouters A, Tran TA, Mouton S, Noben J-P, Gentile L, Smeets K (2018) **A carcinogenic trigger to study the function of tumor suppressor genes in Schmidtea mediterranea** *Dis Model Mech* **11** https://doi.org/10.1242/dmm.032573

van Wolfswinkel JC, Wagner DE, Reddien PW (2014) **Single-cell analysis reveals functionally distinct classes within the planarian stem cell compartment** *Cell Stem Cell* **15**:326–339 https://doi.org/10.1016/j.stem.2014.06.007

Wagner DE, Ho JJ, Reddien PW (2012) **Genetic regulators of a pluripotent adult stem cell system in planarians identified by RNAi and clonal analysis** *Cell Stem Cell* **10**:299–311 https://doi.org/10.1016/j.stem.2012.01.016

Wagner DE, Wang IE, Reddien PW (2011) **Clonogenic neoblasts are pluripotent adult stem cells that underlie planarian regeneration** *Science* **332**:811–816 https://doi.org/10.1126/science.1203983

Wang IE, Wagner DE, Reddien PW (2018) **Clonal Analysis of Planarian Stem Cells by Subtotal Irradiation and Single-Cell Transplantation** *Methods Mol Biol* **1774**:479–495 https://doi.org/10.1007/978-1-4939-7802-1_20

Wenemoser D, Lapan SW, Wilkinson AW, Bell GW, Reddien PW (2012) **A molecular wound response program associated with regeneration initiation in planarians** *Genes Dev* **26**:988–1002 https://doi.org/10.1101/gad.187377.112

Wenemoser D, Reddien PW (2010) **Planarian regeneration involves distinct stem cell responses to wounds and tissue absence** *Dev Biol* **344**:979–991 https://doi.org/10.1016/j.ydbio.2010.06.017

Wurtzel O, Cote LE, Poirier A, Satija R, Regev A, Reddien PW (2015) **A Generic and Cell-Type-Specific Wound Response Precedes Regeneration in Planarians** *Dev Cell* **35**:632–645 https://doi.org/10.1016/j.devcel.2015.11.004

Wurtzel O, Oderberg IM, Reddien PW (2017) **Planarian Epidermal Stem Cells Respond to Positional Cues to Promote Cell-Type Diversity** *Dev Cell* **40**:491–504 https://doi.org/10.1016/j.devcel.2017.02.008

Zeng A *et al.* (2018) **Prospectively isolated Tetraspanin+ neoblasts are adult pluripotent stem cells underlying planaria regeneration** *Cell* **173**:1593–1608 https://doi.org/10.1016/j.cell.2018.05.006

Zhu SJ, Hallows SE, Currie KW, Xu C, Pearson BJ (2015) **A mex3 homolog is required for differentiation during planarian stem cell lineage development** *eLife* **4** https://doi.org/10.7554/eLife.07025

Editors

Reviewing Editor
Carolyn Adler
Cornell University, Ithaca, United States of America

Senior Editor
Didier Stainier
Max Planck Institute for Heart and Lung Research, Bad Nauheim, Germany

Reviewer #1 (Public review):

Summary:

This is a very creative study using modeling and measurement of neoblast dynamics to gain insight into the mechanism that allows these highly potent cells to undergo fate-switching as part of their differentiation and self-renewal process. The authors estimate growth equation parameters for expanding neoblast clones based on new and prior experimental observations. These results indicate neoblast likely undergo much more symmetric self-amplifying division than loss of the population through symmetric differentiation, in the case of clone expansion assays after sublethal irradiation. Neoblasts take on multiple distinct transcriptional fates related to their terminally differentiated cell types, and prior work indicated neoblasts have a high plasticity to switch fates in a way linked to cell cycle progression and possibly through a random process. Here, the authors explore the impact of inhibition of key transcription factors defining such states (ie "fate specifying transcription factors", FSTFs) plus measurement and modeling in the clone expansion assay, to find that inhibition of factors like zfp1 likely cause otherwise zfp1-fated neoblasts to fail to proliferate and differentiation without causing compensatory gains in other lineages. A mathematical model of this process assuming that neoblasts do not retain a memory of prior states while they proliferate, and transition across specified states can mimic the experimentally determined decreased sizes of clones following inhibition of zfp1. Complementary approaches to inhibit more than one lineage (muscle plus intestine) supports the idea that

this is a more general process in planarian stem cells. These results provide an important advance for understanding the fate-switching process and its relationship to neoblast growth.

Overall I find the evidence very well presented and the study compelling. It offers an important new perspective on the key properties of neoblasts. I do have some comments to clarify the presentation and significance of the work.

https://doi.org/10.7554/eLife.100885.1.sa2

Reviewer #2 (Public review):

Summary:

Cell cycle duration and cell fate choice are critical to understanding the cellular plasticity of neoblasts in planarians. In this study, Tamar et al. integrated experimental and computational approaches to simulate a model for neoblast behaviors during colony expansion.

Strengths:

The finding that "arresting differentiation into specific lineages disrupts neoblast proliferative capacities without inducing compensatory expression of other lineages" is particularly intriguing. This concept could inspire further studies on pluripotent stem cells and their application for regenerative biology.

Weaknesses:

However, the absence of a cell-cell feedback mechanism during colony growth and the likelihood of the difference needs to be clarified. Is there any difference in interpreting the results if this mechanism is considered? More explanation and discussion should be included to distinguish the stages controlled by the one-step model from those discussed in this study. Although hnf-4 and foxF have been silenced together to validate the model, a deeper understanding of the tgs-1+ cell type and the non-significant reduction of tgs-1+ neoblasts in zfp-1 RNAi colonies is necessary, considering a high neural lineage frequency.

https://doi.org/10.7554/eLife.100885.1.sa1

Author response:

> ***Reviewer #1:***
>
> *Overall I find the evidence very well presented and the study compelling. It offers an important new perspective on the key properties of neoblasts. I do have some comments to clarify the presentation and significance of the work.*

We thank the reviewer for the positive feedback and plan to improve the presentation of the work.

> ***Reviewer #2:***
>
> *However, the absence of a cell-cell feedback mechanism during colony growth and the likelihood of the difference needs to be clarified. Is there any difference in interpreting the results if this mechanism is considered?*

We will improve the description of the model assumptions and the interpretation of the data on the basis of these assumptions.

> *Although hnf-4 and foxF have been silenced together to validate the model, a deeper understanding of the tgs-1+ cell type and the non-significant reduction of tgs-1+ neoblasts in zfp-1 RNAi colonies is necessary, considering a high neural lineage frequency.*

We will improve the analysis of this result in light of the experimentally determined frequency of the *tgs-1+* neoblast population.

https://doi.org/10.7554/eLife.100885.1.sa0